fire

MDPI

Article

Mechanical Behavior and Ductility of Reinforcing Steel Under High-Temperature Exposure with Different Cooling Methods

Alberto Leal Matilla, Daniel Ferrández *, María Isabel Prieto Barrio and Fernando Israel Olmedo Zazo

Universidad Politécnica de Madrid, E.T.S. de Edificación. Avda. Juan de Herrera, 6, 28040 Madrid, Spain; alberto.leal.matilla@upm.es (A.L.M.); mariaisabel.prieto@upm.es (M.I.P.B.); fi.olmedo.zazo@upm.es (F.I.O.Z.)
* Correspondence: daniel.fvega@upm.es; Tel.: +34-91-06-75291

Abstract

The study of the behaviour of steel reinforcement in high temperatures is essential to understanding the performance of structural concrete after a fire. A special case is presented by steel reinforcements that are exposed to high temperatures after losing all or part of the nominal coating that protects them. In this work, detailed research has been carried out to understand the behaviour of two types of steel, B500SD (carbon) and EN 1.4301 (stainless), exposed to high temperatures. For this purpose, different heating temperatures (450, 800 and 1150 °C) and two types of cooling (rapid in water and slow at room temperature) were used. Mass loss and tensile strength were evaluated, and the ductility indices of these steels were analysed in detail, accompanied by a discussion with a statistical analysis and fractography. The results indicate that stainless steel performs better than carbon steel in a fire. The B500SD reinforcement exhibited a decrease in yield strength of up to 239 MPa (↓ 55%) compared to the reference specimen when heated to 1150 °C. Additionally, it has been observed that rapid cooling results in a more pronounced decrease in ductility in B500SD steel. However, slow cooling led to an increase in ductility in the three indices studied (Cosenza, Creazza and Ortega), with the presence of micro-void coalescence in the fractography corroborating the results. Thus, this research holds great practical interest in decision-making for the selection of structural materials, as it assesses the physical–mechanical behaviour of reinforced concrete after exposure to high temperatures.

Keywords: carbon steel; stainless steel; high-temperature; cooling methods; ductility

Academic Editor: Irina Turku

Received: 5 October 2025
Revised: 20 November 2025
Accepted: 26 November 2025
Published: 27 November 2025

Citation: Leal Matilla, A.; Ferrández, D.; Prieto Barrio, M.I.; Olmedo Zazo, F.I. Mechanical Behavior and Ductility of Reinforcing Steel Under High-Temperature Exposure with Different Cooling Methods. *Fire* **2025**, *8*, 460. https://In Proceedings of the doi.org/10.3390/fire8120460

1. Introduction

The behaviour of reinforced concrete structures in fire situations is a highly relevant issue for construction, as it affects people's safety and the load-bearing capacity of structures [1]. In this regard, it is commonly accepted that after a fire, expert assessments should be carried out to determine the structural capacity of buildings, analysing the level of deterioration of materials and the need for intervention to ensure that the construction as a whole complies with the service conditions for which it was designed [2]. However, although the hot and residual properties of concrete compounds are widely studied [3,4], there are not many studies on steel reinforcement subjected to high temperatures. The aim of this work is to further investigate the behaviour of passive reinforcement subjected to high temperatures, analysing the effect this has on ductility and mechanical strength indices. Table 1 has been compiled to include studies carried out to date that are relevant to the topic under discussion. To this end, a search was conducted in Web of Science using the following search criteria: ((‘ASTM A955′ OR ‘ASTM A615′ OR ‘304 Stainless Steel

Bar') AND ('Cooling' AND ('High Temperature' OR 'Post-Fire') AND ('Mechanical' OR 'Strength')) NOT ("Geopolymer" OR 'Fib*')). In this review of the state of the art, articles published between 2015 and 2025, available in English and available for download in full text, have been selected.

Table 1. Review: Behaviour of passive steel reinforcement under high temperatures and different cooling methods.

Reference	Steel	Temperatures	Heating Rate	Main Results
Ruan et al. (2015) [5]	A615	25, 200, 500, 850 °C.	Heating 5 °C/min, holding 60 min at each temperature; natural (air) or rapid (water) cooling.	Exposure to fire increased corrosion by at least 15% in all cases. The greatest effect occurred at 850 °C with water cooling, where the corrosion rate increased by 60% and mass loss by 40% compared to 850 °C air. Water cooling favoured the formation of martensite.
Gardner et al. (2016) [6]	EN 1.4307 EN 1.4311 EN 1.4162 EN 1.4362	(100 to 1000) °C in intervals of 100 °C.	Steady state: heating at 10 °C/min to the target temperature with 10–15 min stabilisation before the test. Transient state: initial load, then temperature increase at 10 °C/min until failure, without holding time.	Stainless steel reinforcements retained their mechanical properties better than traditional carbon steel, especially above 550 °C. Above 800 °C, there was a significant reduction in strength, although with greater retention compared to carbon steel. Stainless steel showed high ductility after exposure to high temperatures, indicating lower brittleness after cooling.
Rafi et al. (2017) [7]	A615	(100 to 900) °C in intervals of 100 °C.	Heating 5–30 °C/min. Holding 40 min at each temperature and natural cooling in air.	Properties remain virtually stable up to 200 °C. From 200–400 °C, moderate losses in elastic limit and modulus. From 400 °C onwards, very sharp decline. At 700 °C, creep resistance ≈ 15% of the initial value. Presence of 'blue brittleness' between 100–300 °C.
Gao et al. (2018) [8]	EN 1.4301 EN 1.4401	(200 to 1100) °C every 200 °C.	Heating: 20 °C/min. Target temperature maintenance 180 min. Natural cooling or water cooling.	Reduction in elastic limit stress with temperature (30% in EN 1.4301 and 20% in EN 1.4401 at 1100 °C). Modulus of elasticity peaks at +50% at 800 °C. Tensile strength and elongation vary by <10%.
Cadoni & Forni. (2019) [9]	EN 1.4301 EN 1.4401	20 °C Ambient temperatura (200 to 1000) °C every 200 °C.	Heating ≈ 2.8 °C/s (≈170 °C/min) with induction. Maintenance 10 min at target temperature.	As the temperature increases (200–1000 °C), the elastic and ultimate limits of austenitic stainless steel decrease, while plastic deformation and ductility increase, especially above 600 °C.
Sobhan et al. (2020) [10]	B400B	~1000 °C With internal gradients of ~150 °C to 900 °C.	Gas furnace according to ASTM E119. 30 min of heating to maximum temperature; effective time similar to 2 h of actual fire. Natural cooling in a furnace.	The combination of accelerated corrosion (and fire) drastically reduces flexural capacity. Average moment loss of up to 80%. The loss increases with concrete strength and crack score. A correlation is observed between reinforcement mass loss and loss of load-bearing capacity.

Table 1. *Cont.*

Reference	Steel	Temperatures	Heating Rate	Main Results
Quiel et al. (2020) [11]	A615 A706	(300 to 900) °C in 100 °C intervals.	Electric heating to target temperature in 45–90 min; maintenance at constant temperature for 45 min; natural cooling.	Progressive loss of strength and modulus of elasticity at higher temperatures. Ultimate strength is reduced to ~38% at 600 °C. Ultimate and fracture strains decrease to 10–15% of initial values at 600 °C, with slight recovery at higher temperatures. Microstructures show an increase in ferrite and a decrease in pearlite and cementite from 400–500 °C.
Cadoni & Forni. (2021) [12]	B500A	20 °C Ambient temperature (200, 400 and 600) °C.	Heating 3 °C/s (180 °C/min) by induction. Maintenance 10 min for homogeneity. Natural cooling.	Confirms combined sensitivity to temperature and high strain rate. Yield strength drops by 60% and ultimate strength by 70% when reaching 600 °C. Parameters are proposed for the Cowper-Symonds and Johnson-Cook models.
Yang et al. (2021) [13]	A615	>1000 °C, gas fire situation.	Heating according to ISO 834 and holding time until failure of the tested column.	It was verified that fire resistance decreases with higher load ratios or slenderness and improves with larger cross-sectional dimensions. A numerical model was validated to predict temperature, deformations, and residual strength, proposing a simplified calculation method for practical design.
Hager et al. (2021) [14]	B500B	(200, 400, 600, 700, 800 and 1000) °C.	5 °C/min, maintaining the target temperature for 60 min followed by cooling: (a) in an oven without temperature control; (b) rapidly in water.	The mechanical properties of B500B steel remained stable up to 400 °C. Above 600 °C, tensile strength and yield strength decreased significantly, while ductility increased. Rapid cooling resulted in an increase in tensile strength and brittleness. At 1000 °C, the material showed a significant microstructural change, but no loss of strength.
Rehman et al. (2022) [15]	B500B EN 1.4301 EN 1.4401 EN 1.4436	(100 to 900) °C in 100 °C intervals.	10 °C/min, maintaining the target temperature for 60 min followed by cooling (in water, in air or controlled in an oven at 1 °C/min).	Stainless steels retained most of their mechanical properties up to 700 °C, with the cooling method having little effect. At 800 °C and 900 °C, stainless steels experienced a decrease in strength and an increase in ductility due to recrystallisation. B500B carbon steel showed more drastic changes in its mechanical properties and microstructure, with an increase in brittleness when cooled rapidly.

Table 1. *Cont.*

Reference	Steel	Temperatures	Heating Rate	Main Results
Hua et al. (2022) [16]	S30408 cladding layer and HRB400 substrate	20 °C ambient temperature, (300 to 900) °C every 100 °C.	Heating 10 °C/min, maintenance 30 min at each temperature. Natural and water cooling.	Water cooling slightly improves residual strength but reduces ductility. Bimetallic reinforcements offer a clear advantage in reinforced concrete applications, improving corrosion resistance and high tensile energy absorption.
Wu et al. (2023) [17]	EN 1.4301 B500C	20 °C Ambient temperature (200, 400, 600 and 800) °C.	Oven heating according to ISO-834 curve, ≈10 °C/min; temperature maintenance until failure; natural cooling	A calculation formula for the fire resistance of stainless steel–concrete beams is validated, taking into account stud slippage, which increases design safety compared to carbon steel solutions.
Molkens & Rossi. (2024) [18]	B500SD EN 1.4301	Ambient temperature at 1000 °C, with different intervals.	Controlled heating in 100 °C intervals, variable holding times (0.3–4 h). Air and water cooling.	The study proposes a statistical and reliability-based method for assessing the safety of metal structures after a fire. It presents a modified reliability factor and a practical example that facilitates its application in real-life assessments.
Tariq. (2024) [19]	B500B	(250, 550, 850 and 950) °C	Heating at 10 °C/min in accordance with ISO-834. Maintenance at target temperature for 150 min. Cooling for 24 h in a muffle furnace at 1 °C/min.	Different levels of corrosion were applied and then exposed to various temperatures before tensile testing. The results show a significant reduction in strength and ductility, although the modulus of elasticity remains almost unchanged.

After analysing Table 1, several ideas can be drawn from the existing literature. Firstly, various authors have noted that stainless steel performs better than carbon steel at high temperatures [6,15]. In both types of steel, it has been observed that at temperatures above 400–500 °C, mechanical properties begin to be significantly affected. In general terms, at temperatures of 800 °C or higher, passive steel reinforcements exhibit a decrease in their elastic limit strength and ultimate tensile strength [8,14,15]. In the case of stainless steel, at high temperatures, there is an increase in deformation capacity and ductility, especially above 600 °C [9,12]. A loss of mass has also been observed as a result of surface oxides formed on carbon steel during air cooling [10]. This makes it very difficult to perform Vickers microhardness tests, as there is a wide dispersion in the measurements. On the other hand, rapid cooling in water suggests recrystallisation of the surface, which weakens the steel [7,15], which highlights the need to develop new calculation methods and experimental tests on concrete structures after fire damage [12,18].

Several studies are focused on investigating high temperatures in armour with different levels of corrosion [5,10]. These investigations are based on the experimental assumption that steel is exposed in reinforced concrete due to carbonation or chloride corrosion. The greatest loss of strength has been observed in carbon steel reinforcements that have been rapidly cooled in water, which is equivalent to an emergency intervention by firefighters [19]. Finally, other studies, such as those by Betül et al. [20], also utilise finite element

software, including ABACUS or ANSYS, to investigate the behaviour of high temperatures in reinforcement [20]. These theoretical studies often draw on previous experimental research to establish models and incorporate corrections into traditional calculation methods. However, in the coming decades, the future will move towards the development of predictive models based on machine learning and artificial intelligence tools. Understanding the residual mechanical behaviour of steel reinforcement after exposure to elevated temperatures is essential for structural rehabilitation and safety assessment. These results can support post-fire evaluation procedures and contribute to refining code-based approaches (e.g., Eurocode 2 or ACI provisions) for estimating the residual strength and serviceability of reinforced concrete elements.

A typical example of this exceptional risk situation in reinforced concrete structures can be seen in Figure 1. Taken as a reference for the case study analysed in this paper, the B500SD steel reinforcement is exposed in a section of staircase where the concrete has fallen off. It should be noted that this situation corresponds to an exceptional, more severe condition that allows the study to be simplified by evaluating the material's limit behaviour. In practice, the reinforcement bars embedded in the concrete could reach lower temperatures and the cooling rate would be reduced, attenuating the thermal gradients.

Figure 1. Example of exposed rebar in reinforced concrete structures (**a**) and cooling methods (**b**).

The main objective of this work is to analyse the behaviour of passive steel reinforcement subjected to high temperatures and different cooling methods. To this end, two types of steel for use in reinforced concrete structures are studied: B500SD carbon steel and EN 1.4301 stainless steel. To address this main objective, the mass loss in both types of steel after the heating–cooling process is analysed, as well as their mechanical properties through tensile testing and the influence on different ductility indices found in the literature. This represents a distinguishing feature compared to other studies analysed [6,15], as the equivalent steel criterion is employed to calculate three internationally recognised ductility indices: those proposed by Cosenza, Creazza, and Ortega. The study is completed with a fractographic analysis of the steels tested under tension.

2. Materials and Methods

2.1. Materials

Passive reinforcement for reinforced concrete, made of carbon steel (B500SD), was utilised in this research. stainless steel (EN 1.4301) was used in this research. More specifically, 42 steel reinforcements with a length of 360 ± 1 mm and a diameter of 12 mm (21 for each type of steel) were used, whose composition, as provided by the manufacturer, is shown in Table 2. It should be noted that the length of the steel reinforcements was selected to ensure their suitability for the heating furnace used.

Table 2. Composition of the steels used in this research.

B500SD Carbon Steel [21–23]								
Elemento (%)	C ≤0.22	P ≤0.05	S ≤0.05	N ≤0.012	Cu ≤0.8	C Equivalente ≤0.5		
Stainless steel EN 1.4301 [24,25]								
Elemento (%)	C 0.04	P 0.032	S 0.002	Si 0.351	Mn 1.45	Cr 18.145	Ni 8.045	Mo 0.344

With regard to B500SD steel bars, they have a yield strength of (R_e) between 500 and 625 MPa, while the ultimate strength (R_m) of these steel reinforcements is between 575 and 843 MPa. The elongation at break measured over five diameters (A_5) this always exceeds 16% and elongation at maximum load (A_{gt}) reaches at least 7.5%. These values comply with regulations. EN 1992-1-1:2013 [21], ASTM A706 Grade 420/500 [22] and GB/T 201499.2-2018 [23] for steel reinforcement in structural concrete.

On the other hand, EN 1.4301 stainless steel reinforcements, in accordance with ASTM A955/A955M [25], establish a value for the resistance at the elastic limit (R_e) of 215 MPa and an ultimate resistance (R_m) between 500 and 620 MPa. Likewise, according to the manufacturer's specifications, the elongation at break measured over five diameters (A_5) was 33%, and the elongation under maximum load reached 18%, thus complying with the aforementioned regulations and with the standard. GB/2020878-2007 [26].

2.2. Equivalent Steel Criterion

Unlike other studies referenced in the bibliography, this research provides an in-depth examination of the effect that high temperatures have on the ductility indices of the analysed steels. Ductility, defined as the ability of the element to deform without abrupt failure, depends on the interaction between steel and concrete, as well as specific design and load conditions. For this study, the concept of equivalent steel has been employed, understood as steel that offers the same ductility performance as defined in the Eurocode 2 classes (EC-2) and the CEB-FIB Model Code (CM-20) [21,27], even though it may not meet either of these two minimum requirements. For the specific case of this study, three indices corresponding to Cosenza [28], Creazza [29] and Ortega [30] have been analysed.

The Cosenza index (p) is based on the assumption that two steels can be considered equivalent provided that they provide the same rotation capacity to a reinforced concrete section. By developing the model analytically, the following Formula (1) is obtained:

$$p = {\varepsilon_{max}}^{0.73} \cdot \left(\frac{f_{max}}{f_y} - 1 \right)^{0.92} \approx {\varepsilon_{max}}^{0.75} \cdot \left(\frac{f_{max}}{f_y} - 1 \right)^{0.90} \quad (1)$$

where $\frac{f_{max}}{f_y}$ (ratio between the maximum tensile stress of steel f_{max} and the yield strength f_y) represents an index of the strength reserve that steel has after reaching the elastic limit stress; the higher this ratio, the greater the safety margin against breakage. For its part, ε_{max} it represents the elongation of the steel under maximum load, expressed as a percentage and is measured in the test piece after the tensile test.

The Creazza index is based on determining area A^*, defined as the deformation work of the material during the hardening phase, thus incorporating the concept of ductility. This area is comprised of four values: elongation at the elastic limit, ε_y, elongation under

maximum load, ε_{max}, stress at the elastic limit, f_y, and maximum unit stress of steel under tension f_{max}. It is thus determined according to expression (2):

$$A^* = \frac{2}{3} \cdot (f_{max} - f_y) \cdot (\varepsilon_{max} - \varepsilon_y) \quad (2)$$

For its part, the Ortega index identified by the parameter I_d proposes quantifying the ductility of steel as the ratio between toughness (T) and elastic energy (EE). For this purpose, toughness is understood to be the energy per unit volume absorbed by steel during its deformation process, thus coinciding with the sum of the elastic energy and plastic energy obtained after the tensile strength test. This dimensionless parameter is determined using expression (3):

$$I_d = \frac{T}{EE} = 1 + \left(1 + \frac{f_{max}}{f_y}\right) \cdot \left(\frac{\varepsilon_{max}}{\varepsilon_y} - 1\right) \quad (3)$$

Thus, in this study, these indices have been determined for the different types of steel analysed, with the aim of determining the impact of high temperatures and the cooling process experienced on them. These results are accompanied by an ANOVA statistical analysis performed using SPSS Statistics software (IBM, New York, NY, USA) [31].

2.3. Experimental Programme

The experimental programme carried out is outlined in Figure 2.

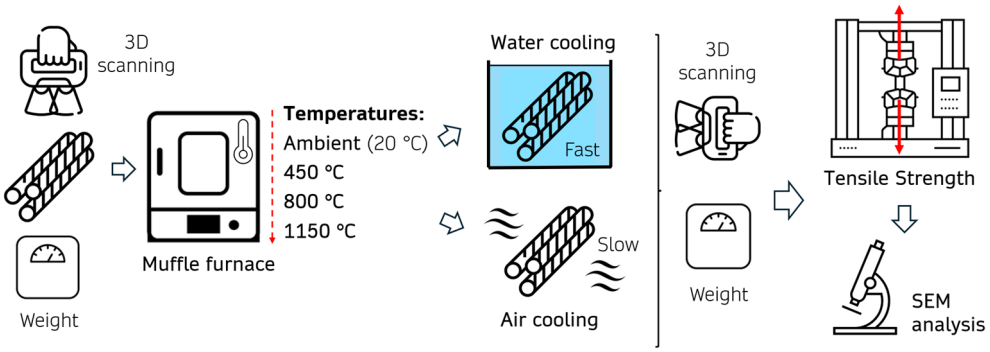

Figure 2. Outline of the experimental programme followed.

The following techniques and methods were used to carry out the experimental campaign developed in this work:

- ***Pre- and post-heating scanning*** (Figure 3a): using a HandySCAN 700 3D scanner from CREAFORM 3D (Quebec, Cánada), which stands out for its high resolution (greater than 0.5 mm), digital image processing speed and metrological accuracy. This scan provides a digitised solid model with the actual morphology of the reinforcement to be tested and detects/quantifies the variations produced in it after the high-temperature heating process. To do this, VX Elements© v.12 software is used for high-resolution image digitisation, which allows the entire solid model or parts of it to be edited, isolated and analysed.
- ***Heating of the reinforcing steel*** (Figure 3b): using an electric muffle furnace from J.P. Selecta (Abrera, Spain). Three heating temperatures were selected in accordance with the Fe-Fe3C diagram: 450 °C and 800 °C, located respectively below and above the eutectoid point (727 °C), and a temperature of 1150 °C close to the eutectic point. In this way, separate temperatures were obtained at regular intervals of 350 °C. Additionally, tests were conducted on the reinforcements at room temperature (20 ± 1 °C). The heating time was 1 h once the target temperature was reached, with a heating rate

of 10 °C/min. In addition, the mass of each bar was determined before and after the heating process using a high-precision electronic balance, model EUROPE 6300 RS (GIBERTINI, Milan, Italy). In any case, the heating regime applied is not aimed at reproducing a standard fire curve, but rather at ensuring controlled thermal exposure in order to assess the residual mechanical behaviour of the steel after the heating and cooling process.

- ***Cooling of the reinforcing steel:*** carried out using two different procedures, known as fast (F) and slow (S). Rapid cooling was achieved by immersing the steel reinforcements in water at a temperature of 9 ± 1 °C after removal from the furnace (simulating the fire extinguishing process [14]), while slow cooling was accomplished by placing the reinforcements in the laboratory until they reached room temperature. In all cases, the procedure was carried out under controlled conditions, ensuring operator safety and avoiding external effects that could influence the study.
- ***Tensile strength test*** (Figure 3c): using an IBERTEST MIB-60/AM universal testing machine (S.A.E. Ibertest, Madrid, Spain). These tests were carried out in accordance with the recommendations and methods outlined in the UNE-EN ISO 15630-1:2019 standard [32]. During the test, a stroke-controlled loading mode was adopted with a speed of 0.34 kN/s. The deformation of the steel reinforcements was measured throughout the process using a high-precision MFA 2 extensometer (Azzano San Paolo, Italy) with a measuring length of 50 mm [33]. Three steel bars were tested for each temperature and cooling method.
- ***Scanning electron microscopy (SEM)***: to perform a fracture analysis using a TESCAN Vega 4 microscope (high/low vacuum) operating at 20 kV with a colour luminescent cathode and two Bruker EDX detectors (30 and 60 mm^2) (Brno, Check Republic). The SEM images were obtained from the steel reinforcements subjected to the highest temperature (1150 °C) for the two types of steel and the two types of cooling, based on the criterion of maximum representativeness of the results and analysing both the central area where the fracture occurred and the surface of the bar.

(a) (b) (c)

Figure 3. Test methods: (**a**) Scanning of the steel reinforcements; (**b**) Heating process; (**c**) Tensile test.

3. Results and Discussion

This section presents the results obtained for the various tests included in the experimental programme, as well as their analysis and critical discussion.

3.1. Morphological Analysis

Firstly, a morphological analysis was conducted on the different steel samples examined in this research. To do this, an initial visual analysis of the reinforcements was performed to extract relevant information on how the heating and cooling processes affect these materials. Figure 4 shows a representative image of each type of bar at each heating temperature, after the cooling process.

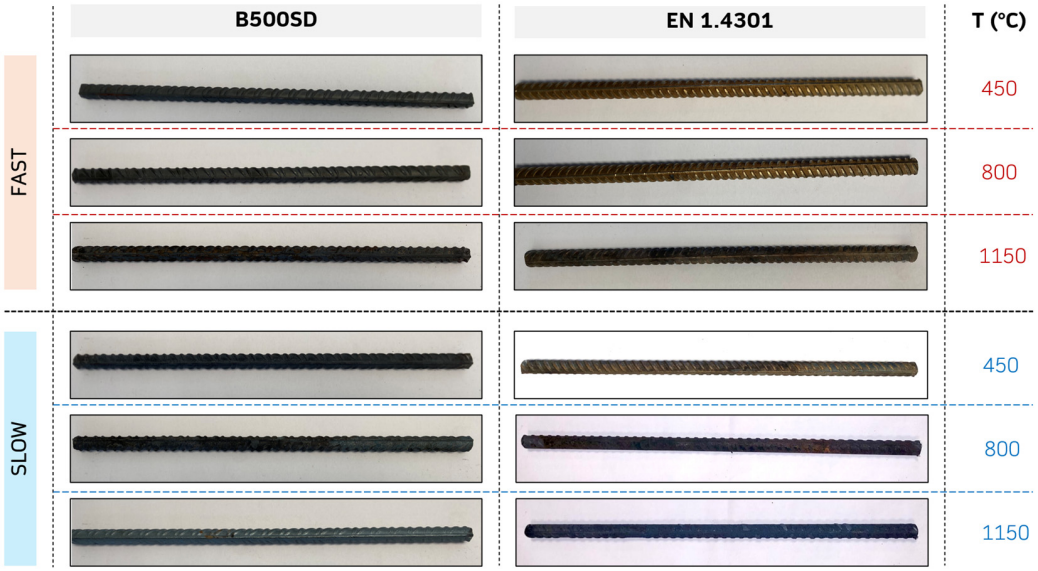

Figure 4. Representative image of each type of bar based on the cooling process and the maximum temperature reached during heating.

As shown in Figure 4, after the heating–cooling process, the B500SD carbon steel reinforcement loses its surface brightness. This effect has been observed in other previous studies, where this increased opacity was attributed to the formation of a surface oxide film, which in turn contributed to a rougher texture [34]. EN 1.4301 stainless steel, on the other hand, experienced a more significant loss of brightness when subjected to a slow cooling process, always at temperatures above 800 °C. Likewise, the surface oxide layer on these steel reinforcements has a golden colour, a consequence of the iron and chromium compounds that form after exposure to these high temperatures [35–37].

Figure 5 shows a representative image of each type of bar, illustrating the variation in its dimensional stability. These images are obtained after scanning each type of steel, both before and after analysis, and reflect the variation with respect to the original diameter of the reinforcement. Knowing these deviations from the original geometry is essential to understanding the material's response to high temperatures, whose deformations can affect the structural integrity of the reinforced concrete components, producing stresses that promote the detachment of the coating, increasing the risk of failure under load and reducing the response time in the event of fire [38]. Additionally, the average variation in percentage mass loss experienced by the different samples studied is documented.

All the steel reinforcements analysed in Figure 5 exhibit a deviation from their original geometry after being subjected to high temperatures. This deviation in the longitudinal direction is more pronounced in samples subjected to a rapid cooling process and affects EN 1.4301 steel reinforcements to a greater extent. Thus, for the maximum temperature tested (1150 °C), the maximum deviation for the stainless steel reinforcements was 9.027 mm, compared to 8.191 mm (↓ 9.26%) obtained in the rapidly cooled carbon steel bars. Likewise, a progressive loss of mass was observed in the steel reinforcements analysed as the heating temperature increased, with the variation experienced by the B500SD steel

reinforcement being much greater. In addition, a greater loss of mass was also observed in the reinforcement subjected to a slow cooling process, which is due to the fact that the steel remains at a high oxygen temperature for a longer period, favouring deeper oxidation [39]. The study of these phenomena is of vital importance for understanding the behaviour that this reinforcement would exhibit once embedded in reinforced concrete. This is because the high temperatures reached in fire situations can cause the steel to expand, generating internal stresses that can lead to the detachment of the nominal coating [40]. In this regard, it is vitally important that the reinforcement does not undergo significant changes in its geometry, without sudden deviations in the longitudinal direction that could constitute preferential points of rupture [41,42].

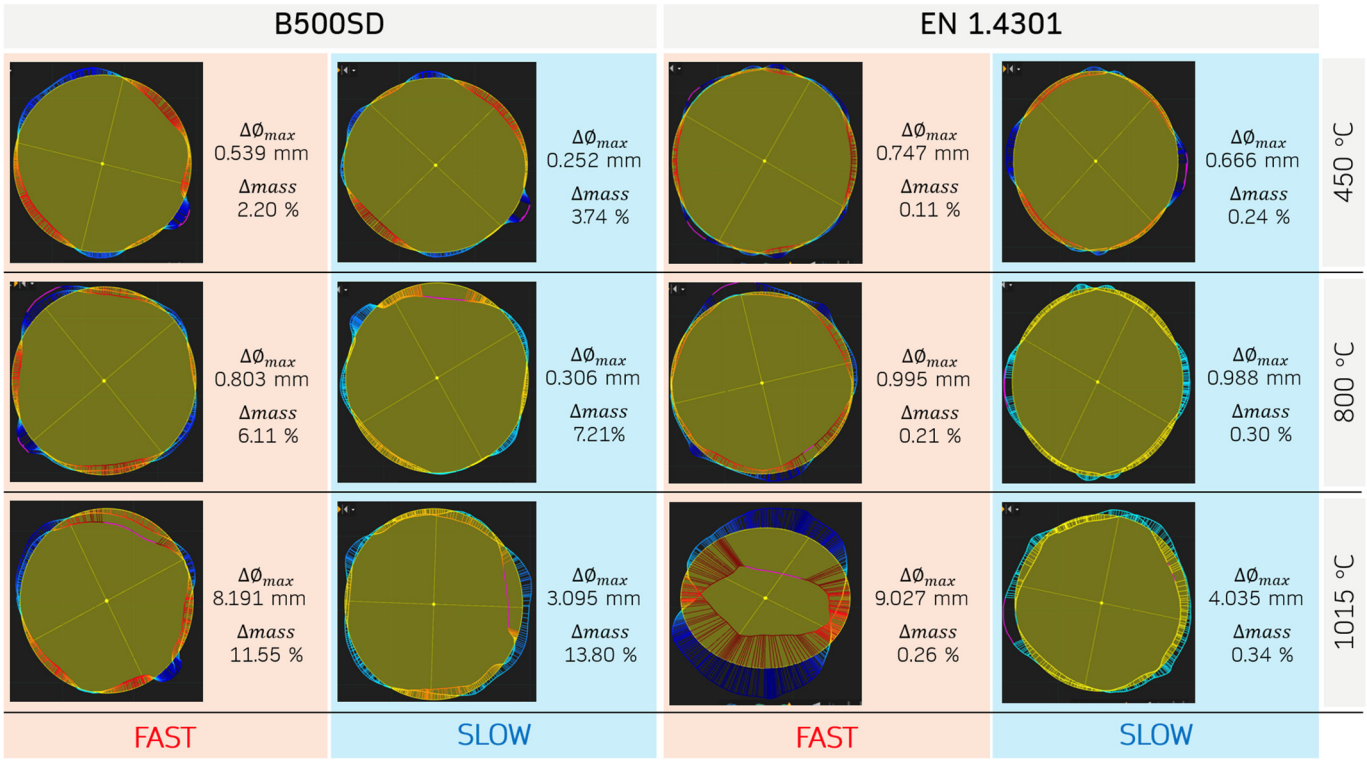

Figure 5. Variation in mass and alteration in the initial geometry of the steel reinforcements studied after the different heating–cooling processes.

3.2. Mechanical Behaviour

This section analyses the mechanical behaviour of the two types of steel studied when subjected to high temperatures and different cooling methods. To this end, the stress-strain (σ–ε) graphs obtained in the experimental tests on the different steel reinforcements analysed are presented first. These graphs are shown in Figures 6 and 7, where the vertical lines, parallel to the slope of the elastic region, indicate the ultimate strain for each type of steel.

Firstly, Figure 6a shows the behaviour of B500SD steel subjected to high temperatures and rapidly cooled in water. It can be seen how this quenching process has a sudden effect on this type of reinforcement. At 450 °C, the strength increases slightly compared to the reference sample, maintaining a similar level of hardness and ductility. However, above 800 °C, the effects of these high temperatures become more visible, with a drastic loss of ductility (reflected in the low deformation until breakage) [43]. This effect is even more noticeable in the steel reinforcements that reached 1150 °C, where both strength and ductility are affected by the severe heating and thermal shock in water. On the other hand, Figure 6b illustrates the effects of slow cooling for this type of steel using the same heating temperatures. As in Figure 6a, at a temperature of 450 °C, the strength increases slightly

compared to the reference. It is when temperatures of 800 °C are reached that a reduction in creep and tensile strength becomes apparent, although greater ductility is observed compared to rapid cooling. The highest temperature of 1150 °C exhibited a significant reduction in strength, although a notable capacity for plastic deformation was maintained prior to fracture. These results show that slow heating favours more ductile behaviour than rapid quenching in water, which is common in cases of fires in reinforced concrete structures [44].

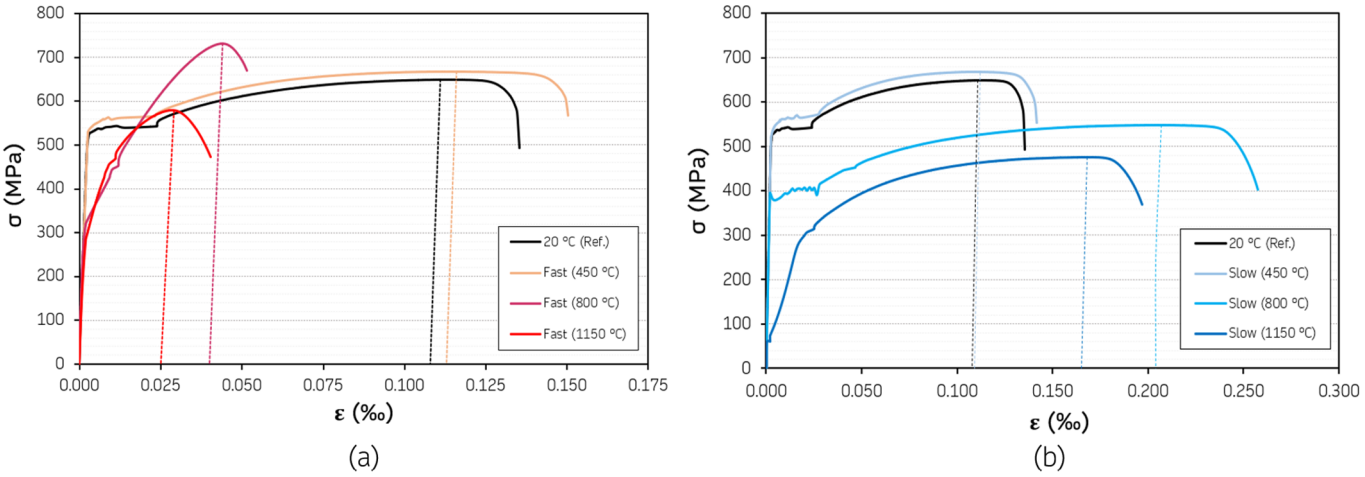

Figure 6. σ–ε graphs for the tensile testing of B500SD steels after different heating/cooling processes, including the line that marks the deformation at the yield limit. (**a**) Fast and (**b**) Cold.

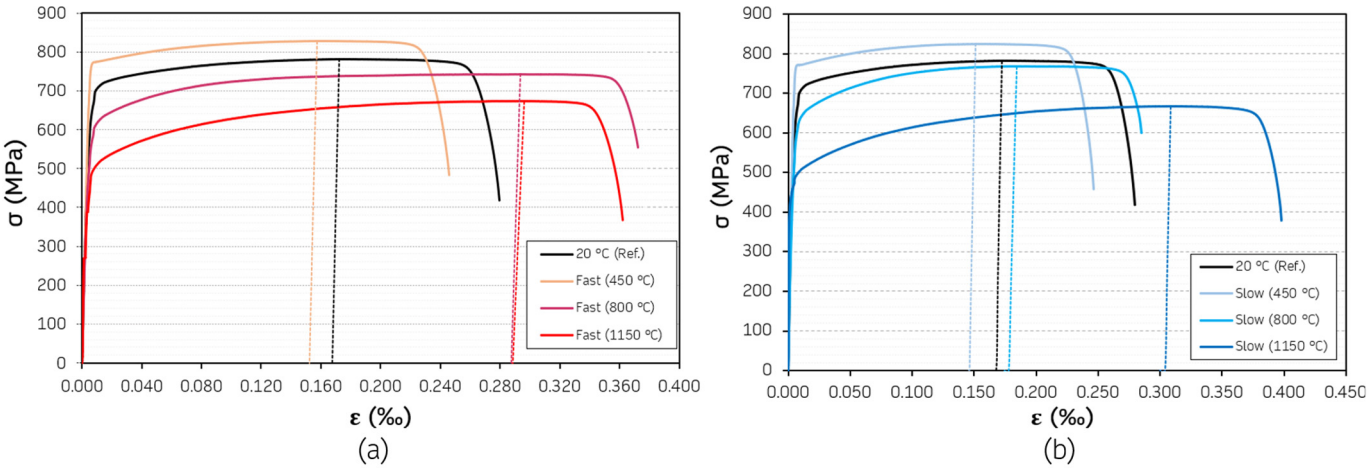

Figure 7. σ–ε graphs for the tensile testing of EN 1.4301 steels after different heating/cooling processes, including the line that marks the deformation at the yield limit. (**a**) Fast and (**b**) Cold.

In stainless steel, rapid cooling after exposure to high temperatures shows a different trend than in carbon steel (Figure 7a). At 450 °C, an increase in tensile strength is observed compared to the reference material; however, ductility at this point is reduced, but remains similar to that of the reference sample. At 800 °C, the material maintains good strength and exhibits greater ductility than carbon steel, reflecting the characteristic microstructural stability of stainless steels. At 1150 °C, although there is a decrease in strength, the plastic deformation capacity remains significant, indicating that water quenching does not induce the drastic embrittlement observed in carbon steels [45]. In the case of slow cooling with this same type of EN 1.4301 steel, it can also be seen how these materials notably retain their properties (Figure 7b). At 450 °C, the material has slightly higher strength values and ductilities very similar to the reference state. At 800 °C, a slight loss of strength

is observed, accompanied by an increase in deformation at break, indicating recovery and partial recrystallisation processes. Finally, at 1150 °C, the strength is reduced more markedly, but the ductility remains high, in contrast to the behaviour of carbon steels [17]. This confirms that stainless steel maintains greater stability under thermal cycles and is a more effective structural solution than carbon steel, although its use is limited due to its significantly higher cost.

Table 3 presents the values extracted from the σ–ε graph for the different mechanical properties of the studied steels, with the aim of gaining a deeper understanding of the effect of these high temperatures.

Table 3. Average values obtained for the different parameters extracted from the σ–ε graphs.

Steel	Cooling	T (°C)	E (GPa)	f_y (MPa)	f_{max} (MPa)	f_y/f_{max}	ε_y (%)	ε_{max} (%)
B500SD	—	20	201.053	530	681	1.286	0.003	0.116
	Fast	450	197.920	515	665	1.291	0.003	0.110
		800	186.200	321	744	2.338	0.002	0.050
		1150	156.445	291	557	1.925	0.003	0.046
	Slow	450	194.675	531	664	1.252	0.002	0.110
		800	196.186	400	548	1.369	0.003	0.189
		1150	117.406	269	497	2.143	0.002	0.163
EN 1.4301	—	20	166.284	325	783	2.410	0.002	0.190
	Fast	450	168.529	345	830	2.410	0.002	0.140
		800	117.844	279	749	2.690	0.002	0.250
		1150	119.982	298	655	2.190	0.002	0.310
	Slow	450	170.642	343	829	2.420	0.002	0.160
		800	116.376	281	768	2.730	0.002	0.200
		1150	103.365	276	622	2.260	0.002	0.320

When analysing Table 3, we see how the modulus of elasticity is strongly affected when steel is subjected to 1150 °C, with the effect caused by high temperatures and slow cooling being more severe. Thus, for B500SD steel subjected to the 'Slow 1150 °C' process, the decrease in E compared to the reference reinforcement is 41.6% (22.2% for the "Fast 1150 °C" case). In the case of stainless steel, the decrease in the modulus of elasticity in the "Slow 1150 °C" process was 37.8% compared to the reference. In all the cases analysed, the yield strength f_y was reduced once temperatures above 450 °C were reached, both in carbon steel and stainless steel. In the case of the maximum load, f_{max} a decrease is also observed, although it is worth noting the increase in rigidity produced by carbon reinforcements with the "Fast 800 °C" process, where greater rigidity and fragility of the sample are observed. Finally, it was observed that deformation of steels occurs when they are subjected to high temperatures. In particular, the parameter ε_y (deformation at the elastic limit) remained constant in the carbon steel reinforcements in both cooling processes.

Since steel reinforcement provides the tensile strength necessary for the mechanical performance of structural concrete, analysing its residual properties after exposure to high temperatures is essential to ensure building safety [46]. These properties depend on multiple factors, such as [47]: chemical composition, manufacturing process, heating time and maximum temperature reached, cooling process, presence of corrosion, and load level of the structure, among others. For this reason, tests such as those presented here, carried out under laboratory conditions, are extremely useful for technicians and professionals in the sector. The behaviour observed in the tensile tests highlights the importance of evaluating the post-fire or post-high-temperature properties of steels, as it

has been observed that exposed B500SD reinforcements undergo significant mechanical degradation and could compromise the stability of the structure, especially when rapid water quenching is used. On the other hand, the effect on EN 1.4301 steel has been less severe, with increased ductility and a lesser loss of load-bearing capacity. In addition, the results of this study can be complemented by those obtained by Zeng et al., which confirmed that exposure times of austenitic steel to high temperatures of 1 h and 7 days had similar effects on the variation of its properties [48].

3.3. Ductility Indices

Figure 8 shows the results for the ductility indices in the different steels subjected to high temperatures and rapid and slow cooling processes.

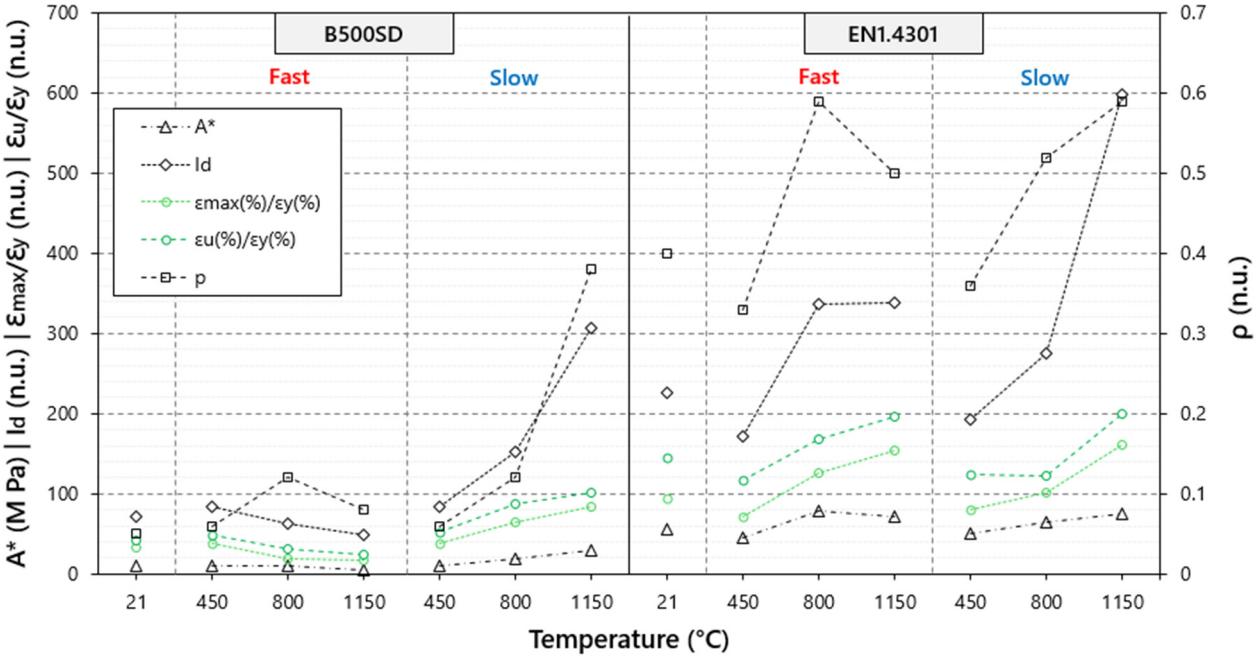

Figure 8. Ductility indices studied, Cosenza, Creazza and Ortega, together with the parameters $\varepsilon_{max}/\varepsilon_y$ and $\varepsilon_u/\varepsilon_y$.

Figure 8 shows a similar trend in the three ductility indices considered: Cosenza, Creazza, and Ortega, as well as in the complementary ductility parameters represented in green, corresponding to $\varepsilon_{max}/\varepsilon_y$ and $\varepsilon_u/\varepsilon_y$. It is clear that the ductility of stainless steels is superior to that of carbon steel in all the tests carried out. In the case of carbon steel, rapid cooling in water resulted in a sharp drop in ductility indices, especially at high heating temperatures (1150 °C). However, for slow cooling, the ductility index values increased progressively as the heating temperature increased. This effect is due to the fact that heat treatment at these high temperatures acts as an annealing process, refining the microstructure into soft phases (ferrite + pearlite), reducing crystalline defects and relieving the internal stresses introduced during the armour forming process [49]. On the other hand, EN 1.4301 steel experiences an increase in ductility in all cases studied, although, as with B500SD steel, heating to 1150 °C and rapid cooling has the most negative effect on these indices. In the case of slow cooling, a progressive trend and increase in ductility were observed with increasing heating temperature. It is essential to note that this type of steel has a microstructure dominated by stable austenite due to its high Ni and Cr content, which enables it to withstand high temperatures very well. When cooled slowly, no brittle phases are formed that severely affect ductility [50]. In short, these processes produce complete

austenitic annealing, which enables the elimination of defects and keeps the austenitic matrix stable and highly ductile.

To complement the discussion of the results shown in Figure 8, a statistical analysis was performed. For this purpose, a one-way analysis of variance (ANOVA) was carried out for the ductility indices, based on the following factors: temperature (levels: 21, 450, 800 and 1150 °C), cooling process (levels: fast and slow) and steel type (levels: B500SD and EN 1.4301). Levene's test revealed heterogeneity of variances and, therefore, it was legitimate to use the Inter-Subject Effects Test. The results obtained are shown in Tables 4 and 5.

Table 4. Descriptive statistics for the ductility indices analysed.

T (°C)	Cooling Process	Steel *	Mean				
			p	A *	I_d	$\varepsilon_{max}/\varepsilon_y$	$\varepsilon_u/\varepsilon_y$
21	—	CS	0.0651	11.5145	60.5508	46.5587	61.7535
		SS	0.0620	14.6325	27.1620	95.0000	146.0932
450	Fast	CS	0.0641	10.7430	60.5508	47.6916	57.7333
		SS	0.0290	7.1205	27.1620	72.5977	116.5981
	Slow	CS	0.0554	9.3640	57.5621	45.9422	62.4000
		SS	0.0215	5.1371	24.3684	79.6667	123.6729
800	Fast	CS	0.1404	10.0535	55.5980	26.8221	33.16670
		SS	0.1122	6.1288	20.0240	126.1667	169.2790
	Slow	CS	0.1186	18.4174	56.5800	75.7695	105.8667
		SS	0.0869	19.8603	22.1962	101.4383	125.4506
1150	Fast	CS	0.0957	7.6933	56.2155	19.1535	19.8667
		SS	0.1685	34.3532	39.0892	154.3330	196.0159
	Slow	CS	0.3007	24.9582	104.3745	65.1780	82.2667
		SS	0.1480	29.4986	38.9565	132.7102	163.9176

* CS = Carbon Steel (B500SD); SS = Stainless Steel (EN 1.4301).

Table 5. Test of inter-subject effects.

Dependent Variable	P			A *			I_d			$\varepsilon_{max}/\varepsilon_y$			$\varepsilon_u/\varepsilon_y$		
Origin *	**df**	**F**	**Sig.**	**df**	**F**	**Sig.**	**df**	**F**	**Sig.**	**df**	**F**	**Sig.**	**df**	**F**	**Sig.**
Corrected Model	13	3.494	0.003	13	4.303	0.001	13	7.53	0.000	13	19.368	0.000	13	19.979	0.000
Intersection	1	87.492	0.000	1	172.18	0.000	1	217.841	0.000	1	897.914	0.000	1	972.723	0.000
Temperature (T)	2	12.608	0.000	2	13.967	0.000	2	7.879	0.002	2	12.168	0.000	2	4.79	0.160
Cooling process (C)	1	0.829	0.370	1	0.289	0.595	1	10.447	0.003	1	2.895	0.101	1	2.917	0.099
Steel type (S)	1	1.589	0.218	1	5.021	0.033	1	29.156	0.000	1	137.766	0.000	1	171.639	0.000
T • C	2	2.718	0.083	2	0.924	0.409	2	4.557	0.019	2	0.358	0.703	2	0.186	0.832
T • S	2	0.017	0.983	2	4.944	0.014	2	0.426	0.657	2	15.468	0.000	2	8.885	0.001
C • S	1	2.983	0.095	1	5.082	0.032	1	14.705	0.001	1	17.407	0.000	1	25.241	0.000
T • C • S	2	2.869	0.074	2	1.49	0.243	2	5.522	0.010	2	6.29	0.006	2	6.966	0.004
R^2			0.62			0.67			0.77			0.90			0.91

* df = degrees of freedom, F = F-distribution, Sig. = Significance ($\alpha = 0.05$).

In Table 4, we can see that stainless steel (SS) generally has higher average values for $\varepsilon_{max}/\varepsilon_y$ and $\varepsilon_u/\varepsilon_y$, reflecting its greater capacity for plastic deformation before fracture, while carbon steel (CS) has more limited ductility, especially at high temperatures (1150 °C). In the study of heating temperatures, at 450 °C, both steels show an increase in ductility (although greater in SS). This behaviour continues to a certain extent at 800 °C, although with greater differences in favour of SS. At 1150 °C, the embrittlement of B500SD steel, which has lower thermal stability, is most noticeable. In terms of cooling methods, the difference for EN 1.4301 steel is not very marked, although CS with slow cooling shows a

notable decrease in ductility. Thus, slow cooling seems to favour ductility conditions when subjecting steels to extreme temperature situations. The T × C interaction indicates that the influence of temperature on ductility strongly depends on the cooling method; slow cooling tends to mitigate the loss of ductility observed at higher temperatures, particularly in the case of stainless steel. The C × S interaction suggests that the two steel types respond differently to cooling, with stainless steel exhibiting a more stable behavior due to its metallurgical composition and higher resistance to thermal degradation. Additionally, the three-way interaction (T × C × S), although of moderate statistical significance, points to a combined effect where temperature, cooling rate, and material type jointly determine the post-fire mechanical performance. These results highlight the importance of considering both material type and cooling conditions in post-fire structural assessments and in the selection of reinforcing steels for fire-resistant design.

For the analysis in Table 5, a significance level of $\alpha = 0.05$ was considered, so p-values lower than this represent a statistically significant effect (with the F parameter measuring the relative magnitude of this effect). Temperature is the most decisive factor in determining ductility, being significant ($p = 0.000$) in the Cosenza, Creazza, and Ortega indices. On the other hand, the cooling process in almost all cases has a p-value > 0.05, so it is not significant on its own. Finally, the steel type factor is significant in all indices ($p = 0.000$), confirming that SS is much more ductile than CS (Table 4). The T × C interaction has a slight effect on Id $\varepsilon_{max}/\varepsilon_y$, and $\varepsilon_u/\varepsilon_y$ therefore, the combination may matter in some scenarios. In contrast, the T × S combination is very significant ($p = 0.000$), reflecting the effect that ductility falls more rapidly at high temperatures in CS. The C × S interaction is less clear, with marginal significance in some indices, suggesting that it slightly reflects the fact that the cooling process has a greater influence on CS than on SS. Finally, the triple interaction T × C × S indicates that the combination of the three factors can modify ductility in certain extreme cases, presenting $p < 0.05$ for the Ortega indices and the factors $\varepsilon_{max}/\varepsilon_y$ and $\varepsilon_u/\varepsilon_y$, It should be noted that the R^2 parameter reflects the fit, such that the model explains between 62% and 91% of the variability depending on the index considered. These values reflect a solid and explanatory model.

3.4. Fractography Study

This section examines the microstructure of the two types of steel used in this research when subjected to the most extreme temperature (1150 °C) and under different cooling methods. This SEM analysis provides in-depth knowledge of the fracture zone of the reinforcements. The SEM images were obtained with the aim of ensuring maximum representativeness of the steel analysed at all times, taking measurements both on the central surface of the bar tested under tension and on the periphery.

3.4.1. B500SD Steel

Firstly, Figure 9 shows the images obtained from the central part of the B500SD reinforcements tested after slow and rapid cooling.

Figure 9 illustrates the effect of high temperatures (1150 °C) on carbon steel, tested for tensile strength after undergoing various cooling processes. At lower magnifications (20×), only the surface texture of the fractured area can be seen, which is slightly more irregular when the bar is subjected to slow cooling. In both cases, the fracture surface appears rough overall, with no well-defined crystalline planes, ruling out the possibility that the samples underwent brittle fracture. At higher magnifications (1000×), cavities and partitions can be seen, which is typical of micro-void coalescence [15]. At the maximum magnification (5000×), surfaces with tear topography are observed, as defined in the UNE 7220:2004 standard [51]. These surfaces have spheroidal and elongated cavities delimited by

partitions, with a typical dome-like morphology (dimples). The microstructural evolution observed shows that rapid cooling with water after exposure to high temperatures favours substantial phase transformation in steel, characterised by the conversion of austenite to martensite, as documented in the literature [52]. In both cooling processes, the formation of micropores is evident during the cooling process, although this effect is more pronounced when the room temperature is reached naturally in air (slowly) [53]. In other words, after slow cooling, larger, elongated/inclined domes and areas where the rings appear open and the cavities are aligned (organ pipe morphology, as defined by the standard [51]) are evident.

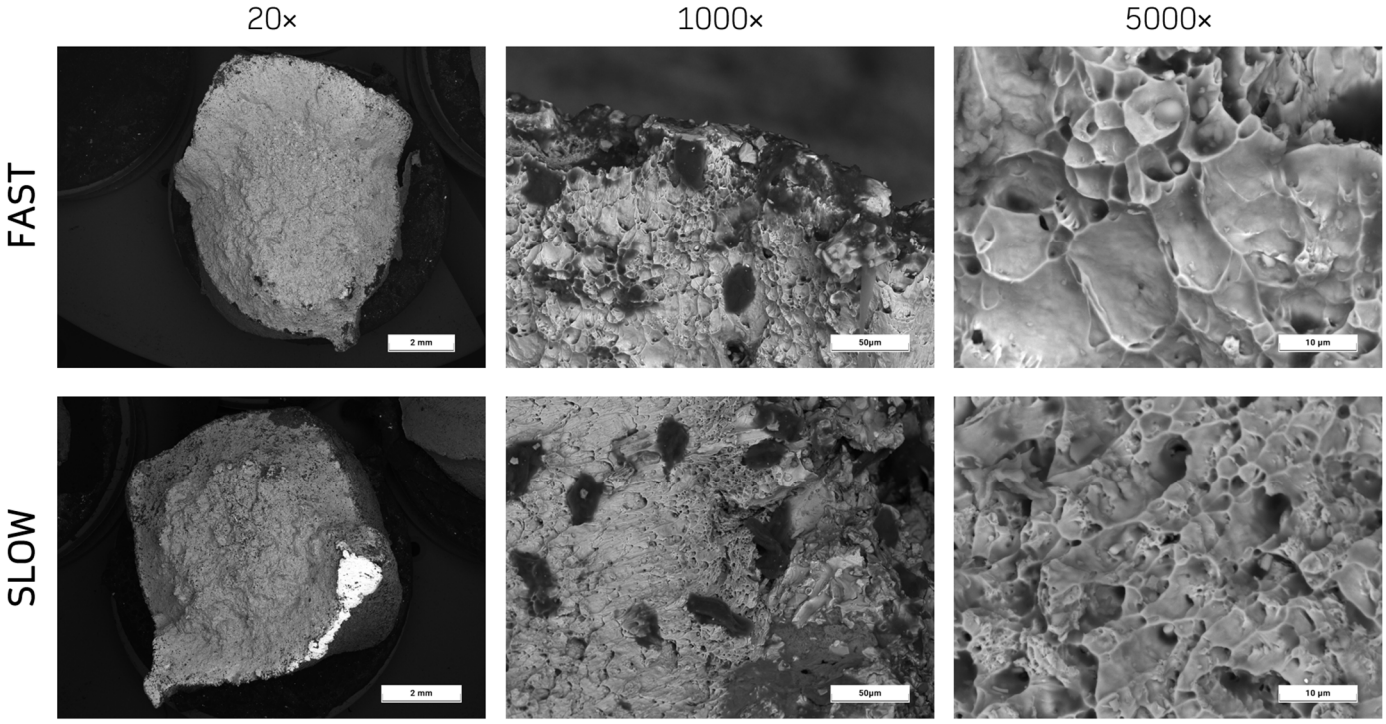

Figure 9. Study of fractography in the central part of B500SD reinforcement bars obtained after tensile testing.

On the other hand, it is also useful to know the effect that the cooling method used has on the exposed surface of the steel bar. For this purpose, the images shown in Figure 10 have been taken.

Figure 10, at low magnification (20×), allows only the area of analysis of the studied reinforcements to be identified, specifically the surface of the passive reinforcement in the area close to the fracture region after the tensile test. At 1000×, a greater appreciation is achieved. The bar subjected to rapid cooling exhibits a polygonal relief with sharp edges and a more pronounced intergranular contour, indicating a greater surface fragility characteristic of tempering processes [54]. On the other hand, the bar with slow cooling shows a mixture of domes and stretched areas (area with tear topography according to UNE 7220:2004 [51], as well as greater porosity that may be caused by the formation of surface oxides and which promotes detachment (as observed in the greater loss of mass reflected in Section 3.1). In rapid cooling at 5000×, grain cleavage facets with steps are produced, sometimes hinting at 'rivers', which is associated with the transcrystalline decohesion mechanism, characterised by greater cracking and fragility [55]. On the other hand, the slow cooling process in these B500SD reinforcements reveals the presence of micro-void coalescence, although greater sponginess and a higher number of dislocations are observed [56].

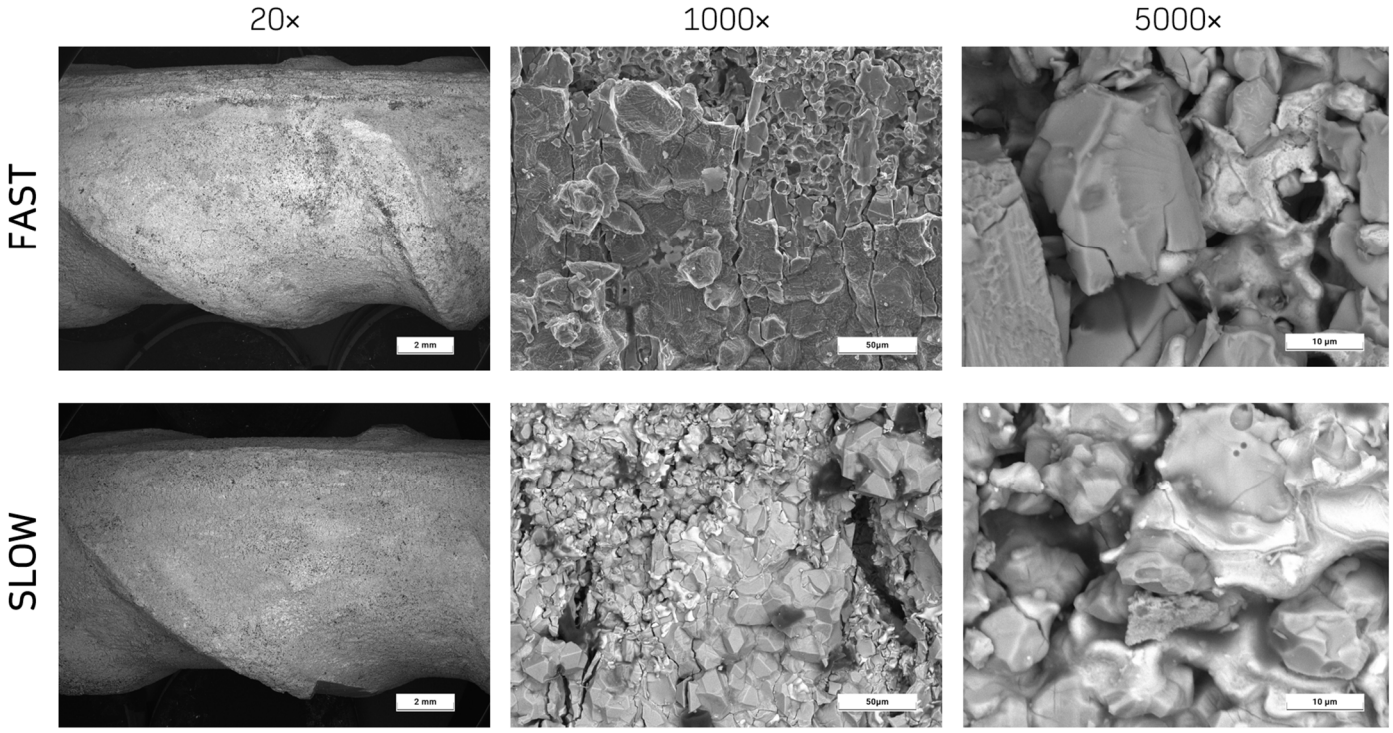

Figure 10. SEM analysis of the surface in the central part of the B500SD reinforcements obtained after the tensile test.

3.4.2. EN 1.4301 Steel

Similarly, the effect of the cooling method on EN 1.4301 reinforcements after being subjected to 1150 °C has been analysed. Figure 11 shows the SEM images obtained from the central area of the bar tested under tension.

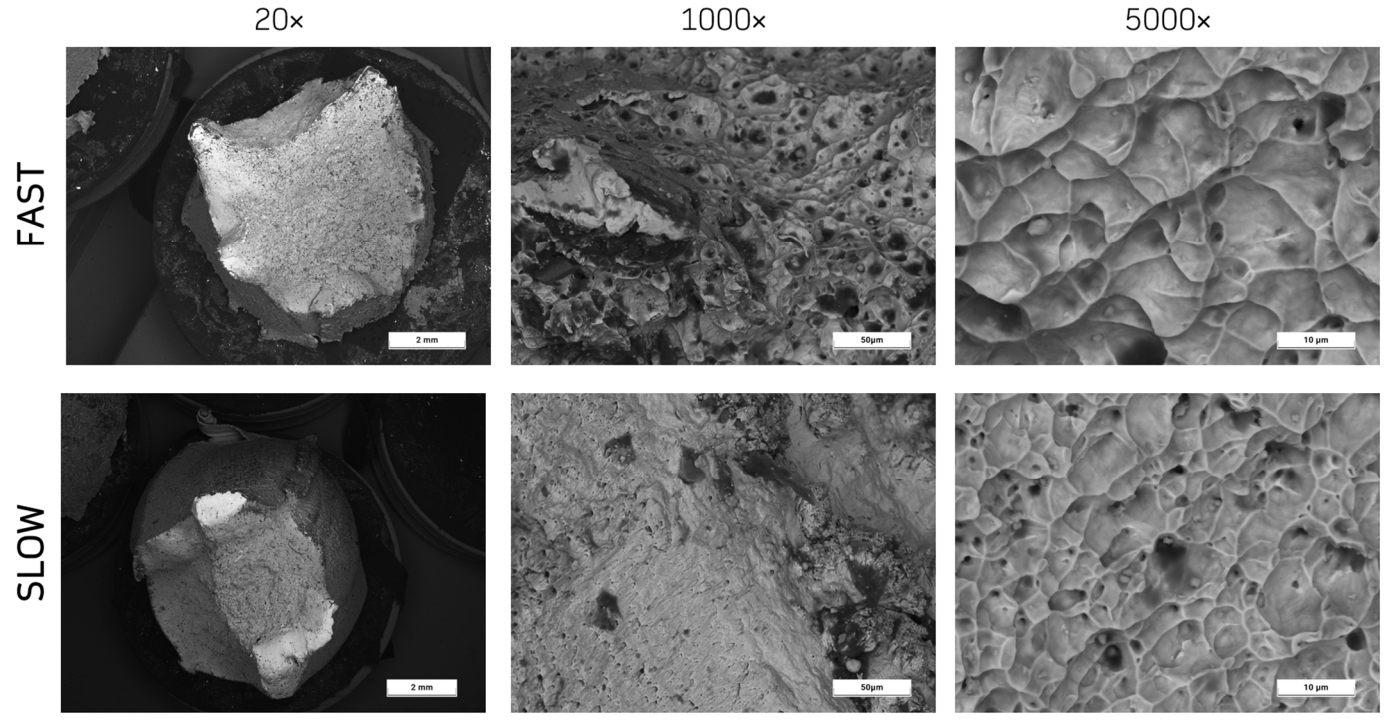

Figure 11. Study of fractography in the central part of EN 1.4301 reinforcement bars obtained after tensile testing.

The images of the armour at 20× magnification included in Figure 11 only show the surface appearance of the fractured face after testing. In both samples, a type of conchoidal fracture typical of tough steels without brittle fracture can be observed, this aspect being more pronounced in the armour subjected to a slow cooling process. At 1000× magnification with rapid cooling, rounded cavities and partitions between these cavities, with a dimpled structure, are clearly visible. At the same magnification with rapid cooling, a more heterogeneous surface is evident, with flat or stretched areas with less developed cavities (stretched zones). In both cases, this type of fracture corresponds to a micro-mechanism of micro-void coalescence, as described in UNE 7220:2004 [51]. At 5000× magnification, both samples exhibit a dominant morphology of equiaxed dimples, typical of ductile fracture [57,58]. The appearance of these domes, which are smaller and more uniform in rapid cooling, indicates a higher deformation rate and homogeneous nucleation of microvoids, whereas in slow cooling, some of these domes are more elongated and have an inclined axis, which is associated with a greater plastic deformation process [59]. In general, large and deep dimples indicate a ductile fracture associated with austenitic regions, while fine dimples are generally related to higher tensile strength and lower ductility, which is attributed to the formation of martensite [60].

Finally, Figure 12 shows the effect on the surface of EN 1.4301 reinforcements subjected to the temperature and cooling methods.

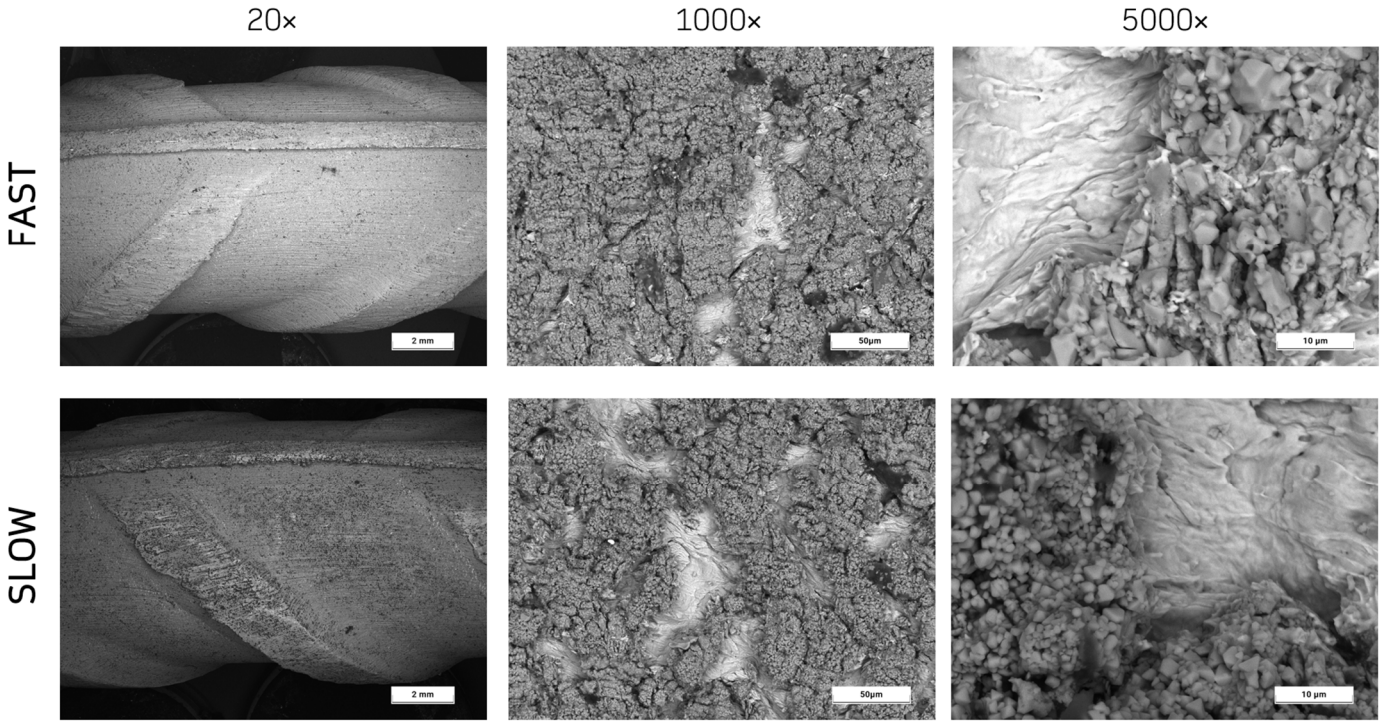

Figure 12. SEM analysis of the surface in the central part of the EN 1.4301 reinforcement bars obtained after the tensile test.

Figure 12, at 20× magnification, shows only the surface of the stainless steel reinforcements analysed, although some roughness can be seen (more pronounced on the slow-cooling bar), reflecting a certain degree of surface oxidation [61]. At an intermediate scale (1000×), both samples have a rough, granular surface with what appear to be microdeposits or oxidation products. In slow cooling, more irregularities are visible, which could be linked to greater precipitation of carbides or secondary phases at grain boundaries, facilitated by slow cooling (a common phenomenon in austenitic stainless steels heated in the critical range) [62]. Under rapid cooling and high magnification (5000×), a surface

with flat and undulating areas appears, which, according to the UNE 7220:2004 standard, can be associated with slip bands and plastic microdeformations. Likewise, under rapid cooling and the same magnification, more defined granular structures predominate, which is compatible with precipitation at grain boundaries and the possible onset of intergranular corrosion [51].

4. Conclusions

The steel embedded in reinforced concrete structures faces risks during fires and can reach high temperatures. This effect on the reinforcement is even more pronounced if the coating has been detached and the steel is exposed to the elements. These elevated temperatures can change the original microstructure and properties of the reinforcement, jeopardising its structural safety and reliability, with the type of steel and cooling process being key variables. This study has considered these factors and provides valuable insights for decision-making in selecting structural materials, particularly regarding the physical–mechanical behaviour of reinforcement after exposure to high temperatures. The main conclusions that can be drawn from this study are as follows:

- High temperatures cause a deviation from the longitudinal axis of the bar, as well as a loss of mass, which are accentuated by the progressive increase in heating temperature. The deviation from the original direction is more pronounced in EN 1.4301 reinforcement bars and during rapid cooling. Consequently, at 1150 °C, the deviation reached up to 9.027 mm from the original diameter. However, the loss of mass is greater in B500SD reinforcement bars and slow cooling (up to 13.80% at a temperature of 1150 °C).
- After the tensile test, it was observed that B500SD steel subjected to high temperatures loses strength and ductility, with this effect being more critical above 800 °C (and particularly noticeable at 1150 °C). In turn, rapid cooling in water causes greater embrittlement in these carbon steel reinforcements, drastically reducing deformation until the material breaks. EN 1.4301 stainless steel, on the other hand, retained its mechanical properties to a greater extent after being subjected to high temperatures, even after undergoing sudden cooling processes.
- The study of ductility indices shows higher values for this property in stainless steels compared to carbon steels. In B500SD reinforcements, rapid cooling causes a marked loss of ductility, while slow cooling favours its recovery through an annealing effect. In the case of EN 1.4301 stainless steel, the stable austenitic microstructure ensures a high deformation capacity even after severe exposure, making it a more resistant material against thermal cycles.
- Fractography tests reveal the coalescence of micro-voids and a tear-like topography in the central part of both types of steel subjected to 1150 °C, indicating a ductile type of fracture. In a superficial analysis, B500SD steel with rapid cooling exhibits a polygonal relief with sharp edges and a more pronounced intergranular contour, indicating greater surface brittleness. On the other hand, in EN 1.4301 steel with slow cooling, irregularities and surface roughness can be observed, which may be attributed to the greater precipitation of carbides or secondary phases at grain boundaries.

Two limitations of this study and future lines of work can be identified. Firstly, it would be interesting to carry out a study of Vickers microhardness in different sections of the armour, although this test is complex because the embrittlement produced in some cases could cause failures and high dispersion in the measurements. Secondly, it would be interesting to conduct a metallographic study on the samples embedded in resin and etched with Nital, so that the effect of the phase changes produced in the steels as a result of these heat treatments can be better appreciated. There are also other recommendations, such as using a greater number of temperatures or replicating the study on reinforcements

of different diameters and types of steel, as these multiple variables are very useful for creating predictive models and obtaining corrected equations for ductility indices. It is also noted that the study could be strengthened by incorporating additional variables into the analysis, such as introducing different levels of corrosion or subjecting the steel bars to various real fire scenarios, using standardized fire curves for the heating process.

Author Contributions: Conceptualization, D.F. and M.I.P.B.; methodology, M.I.P.B. and A.L.M.; software, A.L.M.; validation, D.F., M.I.P.B., A.L.M. and F.I.O.Z.; formal analysis, A.L.M. and D.F.; investigation, A.L.M.; resources, D.F. and M.I.P.B.; data curation, A.L.M.; writing—original draft preparation, A.L.M. and D.F.; writing—review and editing, D.F., M.I.P.B., A.L.M. and F.I.O.Z.; visualization, A.L.M. and F.I.O.Z.; supervision, D.F., F.I.O.Z. and M.I.P.B.; project administration, D.F.; funding acquisition, D.F. All authors have read and agreed to the published version of the manuscript.

Funding: This research received no external funding.

Institutional Review Board Statement: Not applicable.

Informed Consent Statement: Not applicable.

Data Availability Statement: The original contributions presented in this study are included in the article. Further inquiries can be directed to the corresponding author.

Acknowledgments: The authors wish to express their gratitude to Luis E. García Cambronero for his guidance in the interpretation of the images obtained by means of Scanning Electron Microscopy (SEM). They also wish to extend their gratitude to Alfonso Cobo Escamilla for his support and continuous involvement in the development of this research from its inception. Finally, the authors would like to thank Óscar Alfredo Cabrera for his support and selfless assistance in the completion of this article.

Conflicts of Interest: The authors declare no conflicts of interest.

References

1. Felicetti, R.; Gambarova, P.G.; Meda, A. Residual Behavior of Steel Rebars and R/C Sections after a Fire. *Constr. Build. Mater.* **2009**, *23*, 3546–3555. [CrossRef]
2. Sun, B.; Guo, T.; Cheng, J.; Li, W. Smart Multiple Attribute Decision Analysis Framework for Automatic Fire Damage Level Evaluation of Concrete Structures. *J. Build. Eng.* **2025**, *101*, 111987. [CrossRef]
3. Amran, M.; Murali, G.; Makul, N.; Kurpińska, M.; Nehdi, M.L. Fire-Induced Spalling of Ultra-High Performance Concrete: In Proceedings of the A Systematic Critical Review. *Constr. Build. Mater.* **2023**, *373*, 130869. [CrossRef]
4. Qin, D.; Gao, P.K.; Aslam, F.; Sufian, M.; Alabduljabbar, H. A Comprehensive Review on Fire Damage Assessment of Reinforced Concrete Structures. *Case Stud. Constr. Mater.* **2022**, *16*, e00843. [CrossRef]
5. Ruan, T.; Spandley, N.; Johnson, C.; Poursaee, A. The Impact of Fire and Fire Extinguishing Method on the Corrosion Behavior of the Steel Bars in Concrete Pore Solution. *Fire Saf. J.* **2015**, *78*, 196–201. [CrossRef]
6. Gardner, L.; Bu, Y.; Francis, P.; Baddoo, N.R.; Cashell, K.A.; McCann, F. Elevated Temperature Material Properties of Stainless Steel Reinforcing Bar. *Constr. Build. Mater.* **2016**, *114*, 977–997. [CrossRef]
7. Rafi, M.M.; Dahar, A.B.; Aziz, T. High Temperature Mechanical Properties of Steel Bars Available in Pakistan. *J. Struct. Fire Eng.* **2018**, *9*, 203–221. [CrossRef]
8. Gao, X.; Zhang, X.; Liu, H.; Chen, Z.; Li, H. Residual Mechanical Properties of Stainless Steels S30408 and S31608 after Fire Exposure. *Constr. Build. Mater.* **2018**, *165*, 82–92. [CrossRef]
9. Cadoni, E.; Forni, D. Austenitic Stainless Steel Under Extreme Combined Conditions of Loading and Temperature. *J. Dyn. Behav. Mater.* **2019**, *5*, 230–240. [CrossRef]
10. Sobhan, K.; Reddy, D.V.; Martinez, F. Fire Resistance of Corroded High-Strength Structural Concrete. *J. Struct. Fire Eng.* **2021**, *12*, 17–34. [CrossRef]
11. Quiel, S.E.; Irwin, C.H.; Naito, C.J.; Vermaak, N. Mechanical Characterization of Normal and High-Strength Steel Bars in Reinforced Concrete Members under Fire. *J. Struct. Eng.* **2020**, *146*, 04020110. [CrossRef]
12. Cadoni, E.; Forni, D. Mechanical Behaviour of B500A Rebars: Effect of Elevated Temperature and High Strain-Rate. *Fire Saf. J.* **2021**, *122*, 103321. [CrossRef]

13. Yang, D.; Liu, F.; Huang, S.S.; Yang, H. Structural Fire Safety Design of Square and Rectangular Tubed-Reinforced-Concrete Columns. *Structures* **2021**, *29*, 1286–1321. [CrossRef]
14. Hager, I.; Kańka, S.; Maślak, M. Properties of Quenched and Self-Tempered Reinforcing Steel Subjected to High Temperature and Different Cooling Conditions. *J. Struct. Fire Eng.* **2021**, *12*, 141–152. [CrossRef]
15. Rehman, F.U.; Cashell, K.A.; Anguilano, L. Experimental Study of the Post-Fire Mechanical and Material Response of Cold-Worked Austenitic Stainless Steel Reinforcing Bar. *Materials* **2022**, *15*, 1564. [CrossRef]
16. Hua, J.; Wang, F.; Xiang, Y.; Yang, Z.; Xue, X.; Huang, L.; Wang, N. Mechanical Properties of Stainless-Clad Bimetallic Steel Bars Exposed to Elevated Temperatures. *Fire Saf. J.* **2022**, *127*, 103521. [CrossRef]
17. Wu, M.; Fan, S.; Han, Y.; Liang, D.; Xu, Q. Fire-Resistant Design of Stainless Steel-Concrete Composite Beam Considering Slip of Stud Connector. *Thin-Walled Struct.* **2023**, *186*, 110713. [CrossRef]
18. Molkens, T.; Rossi, B. The Post-Fire Assessment of Steel Structures, a Reliability-Based Semi-Probabilistic Approach. *Fire Technol.* **2024**, *60*, 3019–3041. [CrossRef]
19. Tariq, F. Combined Effects of Corrosion and Fire on Load-Carrying Response of Hot-Rolled Steel Reinforcement. *J. Struct. Fire Eng.* **2024**, *15*, 619–644. [CrossRef]
20. Aliş, B.; Yazici, C.; Mehmet Özkal, F. Investigation of Fire Effects on Reinforced Concrete Members via Finite Element Analysis. *ACS Omega* **2022**, *7*, 26881–26893. [CrossRef]
21. *UNE-EN 1992-1-1:2013/A1:2015*; Eurocódigo 2: Concrete Structure Design. Part 1-1: General Rules and Rules for Building Construction. Spanish Association for Standardization (UNE): Madrid, Spain, 2015. Available online: https://www.une.org/encuentra-tu-norma/busca-tu-norma/norma?c=N0055436 (accessed on 30 September 2025).
22. Specification for Deformed and Plain Low-Alloy Steel Bars for Concrete Reinforcement. 2006. Available online: https://store.astm.org/a0706_a0706m-06.html (accessed on 20 October 2025).
23. *GB/T 1499.2-2018*; China Standard English PDF, GB/T 1499.2-2018 Steel for the Reinforcement of Concrete—Part 2: Hot Rolled Ribbed Bars. Standardization Administration of the People's Republic of China: Beijing, China, 2018. Available online: https://es.scribd.com/document/408953345/GBT-1499-2-20180en (accessed on 30 September 2025).
24. *UNE-EN 10088-1:2024*; Stainless Steels—Part 1: List of Stainless Steels. Spanish Association for Standardization (UNE): Madrid, Spain, 2024. Available online: https://www.une.org/encuentra-tu-norma/busca-tu-norma/norma?c=N0073437 (accessed on 30 September 2025).
25. *ASTM A959-19*; Guide for Specifying Harmonized Standard Grade Compositions for Wrought Stainless Steels. ASTM: West Conshohocken, PA, USA, 2019. [CrossRef]
26. *GB/T 20878-2007*; China Standard English PDF, GB/T 20878-2007 Stainless and Heat-Resisting Steels—Designation and Chemical Composition. Standardization Administration of the People's Republic of China: Beijing, China, 2007. Available online: https://es.scribd.com/doc/75201064/GB-T-20878-2007-Stainless-and-Heat-resisting-Steels-Designation-and-Chemical-Composition (accessed on 30 September 2025).
27. *Fib Model Code for Concrete Structures (2020)*; International Federation of Structural Concrete: Lausanne, Switzerland, 2023; ISBN 9782883941755.
28. Cosenza, E.; Greco, C.; Manfredi, G. *An Equivalent Steel Index in the Assesement of the Ductility Performances of the Reinforcement*; CEB Comité Euro international du Béton: Lausanne, Switzerland, 1998; pp. 157–170.
29. Creazza, G.; Russo, S. A New Proposal for Defining the Ductility of Concrete-Reinforcement Steels by Means of a Single Parameter. *Mater. Struct.* **1996**, *29*, 406–410. [CrossRef]
30. Ortega, H. Estudio Experimental de La Influencia Del Tipo de Acero En La Capacidad de Redistribución En Losas de Hormigón Armado. 1999. Available online: https://dialnet.unirioja.es/servlet/tesis?codigo=239117 (accessed on 20 October 2025).
31. IBM. SPSS Statistics. Available online: https://www.ibm.com/es-es/products/spss-statistics?utm_content=SRCWW&p1=Search&p4=43700078923124712&p5=e&p9=58700008629575058&gad_source=1&gclsrc=ds (accessed on 30 September 2025).
32. *ISO 15630-1:2019*; Steel for the Reinforcement and Prestressing of Concrete—Test Methods—Part 1: Reinforcing Bars, Rods and Wire. ISO: Geneva, Switzerland, 2019. Available online: https://www.iso.org/es/contents/data/standard/06/61/66130.html?browse=tc (accessed on 30 September 2025).
33. Extensómetro Longitudinal Medición Pequeñas Extensiones MFA-2. Available online: https://techlabsystems.com/producto/extensometro-longitudinal-medicion-pequenas-extensiones-mfa-2/ (accessed on 7 November 2025).
34. Botella, J.; Almagro, J.; Otero, E.; Hierro, P.; Merino, C. Ageing and High Temperature Oxidation Phenomena in Three High Alloyed Stainless Steels. *Rev. Metal.* **1999**, *35*, 22–32. [CrossRef]
35. Lipiński, T.; Wach, A.; Karpisz, D. Influence the non-metallic inclusions on bending fatigue strength of medium-carbon structural steel melted in an electric furnace. In Proceedings of the 29th International Conference on Metallurgy and Materials, Brno, Czech Republic, 20–22 May 2020. [CrossRef]

36. Wang, M.; Gao, X.; Zhu, C.; Song, L.; Du, L.; Misra, R.D.K.; Zhao, X. Microstructure, Mechanical Properties, and Strain-Hardening Behavior of V–N Microalloyed Pipeline Steels Consisted of Polygonal Ferrite and Acicular Ferrite. *Steel Res. Int.* **2021**, *92*, 2000404. [CrossRef]
37. Tillmann, W.; Ulitzka, T.; Dahl, L.; Wojarski, L.; Ulitzka, H. An Investigation of the Influence of Integration of Steel Heat Treatment and Brazing Process on the Microstructure and Performance of Vacuum-Brazed Cemented Carbide/Steel Joints. *Weld. World* **2022**, *66*, 1053–1066. [CrossRef]
38. Leal Matilla, A.; Ferrández, D.; Prieto Barrio, M.I.; Varum, H. Systematic Review on the Behaviour of Carbon and Stainless Steel Reinforcing Bars in Buildings Under High Temperatures. *Buildings* **2025**, *15*, 1539. [CrossRef]
39. Haapakangas, J.; Airaksinen, S.; Heikkinen, E.P.; Fabritius, T. Oxidation of Carbon Steels in Novel Reheating Conditions: Changes to Oxidation Kinetics. *Metall. Mater. Trans. B Process Metall. Mater. Process. Sci.* **2025**, *56*, 3762–3773. [CrossRef]
40. Jelani, M.; Li, Z.; Shen, Z.; Hassan, N.U.; Sardar, M. Mechanical Response and Failure Evolution of 304L Stainless Steel under the Combined Action of Mechanical Loading and Laser Heating. *Metals* **2018**, *8*, 620. [CrossRef]
41. Yao, X.; Qin, P.; Guan, J.; Li, L.; Zhang, M.; Gao, Y. Residual Mechanical Properties and Constitutive Model of High-Strength Seismic Steel Bars through Different Cooling Rates. *Materials* **2021**, *14*, 469. [CrossRef]
42. Ba, G.; Weng, X.; Liu, C.; Miao, J. Bond strength of corroded reinforcements in concrete after high-temperature exposure. *Constr. Build. Mater.* **2021**, *270*, 121400. [CrossRef]
43. Thongchom, C.; Kongwat, S.; Jaitrong, J.; Keawsawasvong, S.; Bui, L.V.H.; Stitmannaithum, B.; Mousa, S. Effect of Elevated Temperatures on Mechanical Properties of Spliced and Non-Spliced Steel Reinforcements: Experimental Study. *Buildings* **2023**, *13*, 1419. [CrossRef]
44. Lapuebla-Ferri, A.; Pons, D.; Romero, M.L. Load and Temperature Influence on the Post-Fire Mechanical Properties of Steel Reinforcements. *J. Constr. Steel Res.* **2021**, *185*, 106866. [CrossRef]
45. Chi, J.; Peng, P. Using the microstructure and mechanical behavior of steel materials to develop a new fire investigation technology. *Fire Mater.* **2017**, *41*, 864–870. [CrossRef]
46. Kog, Y.C. Practical Guide for the Assessment and Repair of Fire-Damaged Concrete Building Structures. *Pract. Period. Struct. Des. Constr.* **2021**, *26*, 04021010. [CrossRef]
47. Maraveas, C.; Fasoulakis, Z.; Tsavdaridis, K.D. Post-Fire Assessment and Reinstatement of Steel Structures. *J. Struct. Fire Eng.* **2017**, *8*, 181–201. [CrossRef]
48. Zeng, D.; Lo, K.H.; Cheang, K.H.; Lai, J.K.L. Remaining Strengths and Pitting Resistance of AISI 316 after a Fire Attack: Implications for Use as Concrete Rebars. *J. Mater. Eng. Perform.* **2013**, *22*, 1481–1489. [CrossRef]
49. Singh, S.; Samir, S.; Kumar, K.; Thapa, S. Effect of Heat Treatment Processes on the Mechanical Properties of AISI 1045 Steel. *Mater. Today Proc.* **2021**, *45*, 5097–5101. [CrossRef]
50. Järvenpää, A.; Jaskari, M.; Kisko, A.; Karjalainen, P. Processing and Properties of Reversion-Treated Austenitic Stainless Steels. *Metals* **2020**, *10*, 281. [CrossRef]
51. *UNE 7220:2004*; Microfractografía de Materiales Metálicos. Terminología. Spanish Association for Standardization (UNE): Madrid, Spain, 2004. Available online: https://www.une.org/encuentra-tu-norma/busca-tu-norma/norma?c=N0030645 (accessed on 1 October 2025).
52. Yin, H.; Zhao, E.; Zhao, M.; Ji, B.; Zhang, X. Post-Fire Fatigue Crack Growth Behavior of S355J2W Weathering Steel: Effects of Fire-Exposure Temperature and Cooling Methods. *Constr. Build. Mater.* **2025**, *493*, 143203. [CrossRef]
53. Han, R.; Yang, G.; Fu, Z.; Xu, D.; Xu, Y.; Zhao, G. Effect of Low-Temperature Hot Rolling on the Microstructure and Mechanical Properties of Air-Cooling Medium Manganese Martensitic Wear-Resistant Steel. *Mater. Charact.* **2023**, *203*, 113139. [CrossRef]
54. Papin, J.; Delattre, J.B.; Flament, J.L.; Marini, B.; Joly, P.; Mathieu, J.P.; Vincent, L.; Gourgues-Lorenzon, A.F. Effects of Quenching and Tempering Conditions of a Low-Alloy Pressure Vessel Steel (A508 Gr.3) on Its Brittle Fracture Initiation and Toughness. *Procedia Struct. Integr.* **2025**, *68*, 727–733. [CrossRef]
55. Xiao, N.; Fei, J.; Li, M.; Zhou, J.; Jia, T. Design of Cooling Route for Carbide-Free Bainitic Rail Steels and Resultant Microstructures and Properties. *Mater. Sci. Eng. A* **2024**, *891*, 145936. [CrossRef]
56. Tao, P.; Yu, H.; Fan, Y.; Fu, Y. Effects of Cooling Method after Intercritical Heat Treatment on Microstructural Characteristics and Mechanical Properties of As-Cast High-Strength Low-Alloy Steel. *Mater. Des. (1980–2015)* **2014**, *54*, 914–923. [CrossRef]
57. Das, A.; Tarafder, S. Geometry of Dimples and Its Correlation with Mechanical Properties in Austenitic Stainless Steel. *Scr. Mater.* **2008**, *59*, 1014–1017. [CrossRef]
58. Suárez Ocaño, P.; Ávila Calderón, L.A.; Agudo Jácome, L.; Rehmer, B.; Mohr, G.; Evans, A.; Skrotzki, B. Effect of 700–900 °C Heat Treatments and Room and High Temperature Tensile Deformation on the Microstructure of Laser Powder Bed Fused 316L Stainless Steel. *Mater. Sci. Eng. A* **2025**, *939*, 148469. [CrossRef]
59. Nishio, R.; Umetani, T.; Nakamura, Y.; Sasaki, T.T.; Shibata, A. Effect of Cooling Rate after High-Temperature Heating on the Ductility of 19Cr-0.020C-0.015N-0.4Nb Stabilized Ferritic Stainless Cast Steel. *Mater. Sci. Eng. A* **2025**, *945*, 148952. [CrossRef]

60. Siahaan, A.S.; Ishihara, S.; Sasaki, Y.; Kawai, H.; Nagasaka, T. Thermo-Viscoelastic Mechanical Behavior and Fractography Analysis of Lean Duplex Stainless Steel SUS821L1. *Results Eng.* **2025**, *27*, 105911. [CrossRef]
61. Su, M.; Zhao, J.; Tian, Z.; Gu, C. Short-Term Oxidation Behavior of 304 Stainless Steel in N_2-21 Vol%O_2 Environment between 900 and 1200 °C. *Corros. Sci.* **2022**, *208*, 110612. [CrossRef]
62. Ivanova, T.; Kořenek, M.; Mashlan, M.; Fryšák, M. Investigation of Surface Oxidation of Cast Austenitic 304 Stainless Steel at High Temperatures. *Metals* **2025**, *15*, 748. [CrossRef]